

Towards Better Long-range Time Series Forecasting using Generative Adversarial Networks

Shiyu Liu, Mehul Motani

Department of Electrical and Computer Engineering
National University of Singapore
shiyu_liu@u.nus.edu, motani@nus.edu.sg

Abstract

Accurate long-range forecasting of time series data is an important problem in many sectors, such as energy, healthcare, and finance. In recent years, Generative Adversarial Networks (GAN) have provided a revolutionary approach to many problems. However, the use of GAN to improve long-range time series forecasting remains relatively unexplored. In this paper, we utilize a Conditional Wasserstein GAN (CWGAN) and augment it with an error penalty term, leading to a new generative model which aims to generate high-quality synthetic time series data, called CWGAN-TS. By using such synthetic data, we develop a long-range forecasting approach, called Generative Forecasting (GenF), consisting of three components: (i) CWGAN-TS to generate synthetic data for the next few time steps. (ii) a predictor which makes long-range predictions based on generated and observed data. (iii) an information theoretic clustering (ITC) algorithm to better train the CWGAN-TS and the predictor. Our experimental results on three public datasets demonstrate that GenF significantly outperforms a diverse range of state-of-the-art benchmarks and classical approaches. In most cases, we find a 6% - 12% improvement in predictive performance (mean absolute error) and a 37% reduction in parameters compared to the best performing benchmark. Lastly, we conduct an ablation study to demonstrate the effectiveness of the CWGAN-TS and the ITC algorithm.

1 Introduction

Short-range forecasting of time series data has been able to provide some useful information, but its scope of application is limited (Granger and Newbold 2014; Bica et al. 2020). In most applications, long-range forecasting of time series data is preferred as it allows more time for early intervention and planning opportunities (Alvarez et al. 2010; Azad, Mekhilef, and Ganapathy 2014). For example, long-range forecasting of patient’s vital signs effectively gives clinicians more time to take action and may reduce the occurrence of potential adverse events (Choi and et al 2016; Jarrett et al. 2021).

One critical issue affecting the long-range forecasting is that the predictive performance (e.g., N -step ahead) becomes worse as N grows. One practical approach to address this problem is to use synthetic data to shorten the prediction horizon N . For example, in iterative forecasting (Mar-

cellino, Stock, and Watson 2006; Hamzaçebi, Akay, and Kuntay 2009), the previous predictions are used together with the original data to evaluate the next prediction. However, the synthetic data (i.e., previous predictions) generated in such a recursive and supervised manner is susceptible to error propagation (Sorjamaa and et al 2007; Weigend and Gershenfeld 2018). Overall, the quality of synthetic data is the key to improving long-range forecasting. In recent years, the success of Generative Adversarial Networks (GAN) (Goodfellow and et al 2014) in replicating real-world content has inspired numerous GAN based architectures (Frid-Adar et al. 2018a,b; Shin et al. 2018; Bowles et al. 2018) to generate synthetic data for different purposes. However, the utilization of such synthetic data to improve long-range forecasting remains unexplored. In this paper, we contribute to the area of long-range forecasting as follows.

1. We augment a conditional Wasserstein GAN (CWGAN) with an error penalty term. This new architecture, called CWGAN-TS, aims to generate accurate synthetic time series data which preserves the temporal dynamics between the conditioning input and the generated data.
2. We develop a long-range forecasting approach called Generative Forecasting (GenF) which consists of three components: (i) CWGAN-TS to generate synthetic data for next few time steps. (ii) a predictor to make long-range predictions based on generated and observed data. (iii) an information theoretic clustering (ITC) algorithm to better train the CWGAN-TS and the predictor.
3. We conduct experiments on three public time series datasets and our results demonstrate that GenF significantly outperforms a diverse range of state-of-the-art benchmarks and classical approaches. In most cases, we find a 6% - 12% improvement in predictive performance (mean absolute error) and a 37% reduction in parameters compared to the best performing benchmark.

2 Background on Time Series Forecasting

In time series forecasting, we use an observation window of historical data to predict the future value (see Fig. 1). Let M denote the observation window length and N denote the prediction horizon. For methods that contain generative models, it has a synthetic window. Let $X_i \in \mathbb{R}^K$ be the observation at the i_{th} time step, where K is the number of features. The prediction horizon is N , indicating that we plan to make pre-

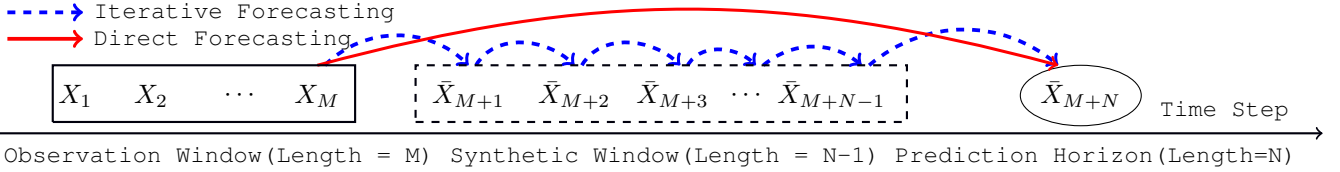


Figure 1: Direct/Iterative Forecasting via Observation/Synthetic Window and Prediction Horizon.

dictions N time steps ahead, i.e., at time step $t + N$. Next, in Section 2.1, we discuss related work and the application of GAN-based models. In Section 2.2, we shortlist four classical models and three strong baselines for comparison.

2.1 Related Work

Early methods using neural networks to perform long-range forecasting include (Nguyen and Chan 2004; Al-Saba and El-Amin 1999). For example, Nguyen and Chan (2004) propose a group of neural networks to make predictions at different time steps. More recently, several works (Yu et al. 2017; Lai et al. 2018; Guen and Thome 2019; Sen, Yu, and Dhillon 2019; Rangapuram et al. 2018) attempt to improve the long-range forecasting by proposing new architectures. For example, Yu et al. (2017) propose a Long Short-Term Memory (LSTM) (Hochreiter and Schmidhuber 1997) based Tensor-Train Recurrent Neural Network as a module for sequence-to-sequence framework (Sutskever, Vinyals, and Le 2014), called TLSTM. Moreover, Lai et al. (2018) propose a Long- and Short-term Time-series network (LSTNet) which incorporates with an attention-based layer and autoregressive models to minimize a customized loss function inspired by support vector regression (SVR) (Cortes and Vapnik 1995). More recently, Li et al. (2019) propose a transformer based model called LogSparse, aiming to improve long-range forecasting with fine granularity and strong long-term dependencies. One more interesting work to mention is (Ahmed, Atiya, and Gayar 2007), which combines Gaussian processes (Rasmussen 2003) and neural networks to improve the forecasting performance. Overall, all these methods can be classified into two classes: direct and iterative forecasting (Bontempi, Taieb, and Le Borgne 2012).

In direct forecasting, the model is trained to directly make predictions for the prediction horizon N (see the solid line in Fig. 1). The advantage is that the models trained for different values of N are independent from each other and hence, immune to the error propagation. However, as N grows, direct forecasting tends to provide forecastings with low bias but high variance as it does not leverage the dependencies between the generated synthetic data (Hamzaçebi, Akay, and Kutay 2009; Taieb et al. 2012). This can be seen by considering an example where the best forecast is a linear trend. In this case, direct forecasting may yield a broken curve due to its mechanism (Bontempi 2008; Bontempi and Taieb 2011).

In iterative forecasting, the model is trained to make predictions for the next time step only. Then, the same model will be used over and over again and previous predictions are used together with the past observations as new inputs to make predictions for the next time step (see the dashed line in Fig. 1). This process is recursively repeated N times to make predictions for the next N time steps. The previ-

ous predictions can be considered as synthetic data with a synthetic window length = $N - 1$. However, the synthetic data generated in such a supervised and recursive manner is more susceptible to error propagation, meaning that a small error in the current prediction becomes a larger error in subsequent predictions, leading to low variance but high bias forecastings (Sorjamaa and et al 2007; Bontempi, Taieb, and Le Borgne 2012). Overall, the quality of synthetic data is the key to improving long-range forecasting.

Recently, GAN (Goodfellow and et al 2014) based neural networks have demonstrated promising results in many generative tasks (Haidar and Rezagholizadeh 2019; Dong et al. 2018). The first GAN applied to time series data is C-RNN-GAN (Mogren 2016) which takes random noise as input and uses LSTM as both the generator and discriminator. One follow-up work, RCGAN (Esteban, Hyland, and Rätsch 2017) makes use of the conditioning information to generate synthetic medical data. Along the way, many works have explored generating synthetic data to address various problems (Frid-Adar et al. 2018a; Bowles et al. 2018; Yoon, Jarrett, and van der Schaar 2019). For example, Frid-Adar et al. (2018) make use of synthetic data augmentation to improve the classification results, and Bowles et al. (2018) mix the synthetic data with training data to enhance the model’s predictive ability. More recently, Yoon, Jarrett, and van der Schaar (2019) propose TimeGAN which trains predictive models to perform one-step ahead forecasting. However, to the best of our knowledge, none of them have considered using the synthetic data generated by the GAN based architecture, to improve long-range forecasting.

2.2 Benchmark Methods

The taxonomy above suggests that most existing methods can be classified as either direct or iterative forecasting. This motivates us to use both direct and iterative forecasting as benchmark methods. As mentioned above, classical models such as LSTM, Autoregressive Integrated Moving Average (ARIMA) (Box and Pierce 1970), SVR, and Gaussian Process Regression (GPR) (Rasmussen 2003) are used to form the core of many state-of-the-art methods. Hence, we use these four classical models to implement both direct and iterative forecasting. In addition, three strong baselines described above: TLSTM (seq2seq based model), LSTNet (attention based model), and LogSparse (transformer based model), are also selected for comparison as they are reported to provide outstanding long-range forecasting performance (Yu et al. 2017; Lai et al. 2018; Cheng, Huang, and Zheng 2020). Moreover, the authors of these methods have provided clear and concise source code, allowing us to correctly implement and tune these learning algorithms.

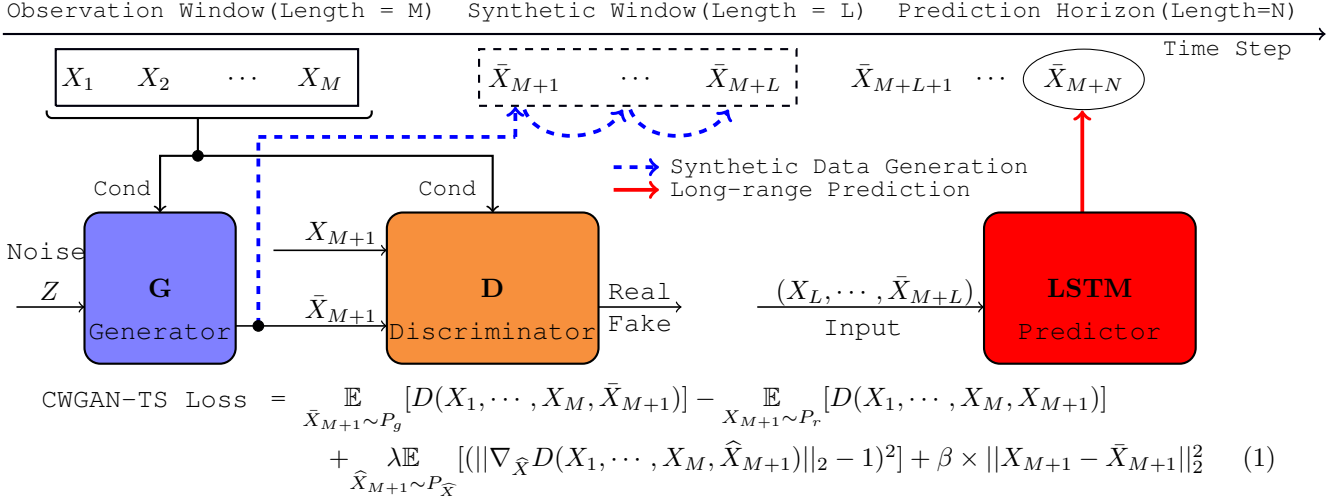


Figure 2: Illustration of GenF (Left: CWGAN-TS [G: Generator, D: Discriminator]; Right: LSTM based Predictor).

3 Generative Forecasting

To improve long-range forecasting, we develop an approach called Generative Forecasting (GenF) as illustrated in Fig. 2. It can be seen that GenF contains two steps: (i) Synthetic Data Generation for the next L time steps (see the blue dashed line). (ii) Long-range Prediction via past observations and generated synthetic data (see the red solid line).

We note that GenF does not belong to either direct or iterative forecasting. The **key difference** is that GenF leverages synthetic data to shorten the predictive horizon, but its synthetic window (length = L) is much shorter than the synthetic window (length = $N - 1$) of iterative forecasting. Next, we describe the three components of GenF: (i) the CWGAN-TS synthetic data generator, (ii) the LSTM based predictor and (iii) the ITC algorithm. Lastly, we summarize the advantage of GenF over direct/iterative forecasting.

3.1 The CWGAN-TS Synthetic Data Generator

We propose a Conditional Wasserstein GAN with Gradient and Error Penalty (Arjovsky, Chintala, and Bottou 2017; Mirza and Osindero 2014; Gulrajani and et al 2017), called CWGAN-TS, aims to generate synthetic time series data. As shown in Fig. 2, The Gaussian noise Z will be used as an input to the CWTAN-TS and past observations will be used as a condition to direct the generation of synthetic data for the next time step (i.e., \bar{X}_{M+1}) (Mirza and Osindero 2014). Next, the synthetic data will be evaluated by the discriminator given the past observations as a condition. The configuration of the CWGAN-TS is provided in Table 1 and the loss function is summarized in (1), where $X_{M+1} \sim P_r$ is the real data at time step $M + 1$, $\bar{X}_{M+1} \sim P_g$ is the generated data for time step $M + 1$ and \hat{X}_{M+1} is sampled from \bar{X}_{M+1} and X_{M+1} with ϵ uniformly sampled between 0 and 1, i.e., $\hat{X}_{M+1} = \epsilon \bar{X}_{M+1} + (1 - \epsilon) X_{M+1}$ with $0 \leq \epsilon \leq 1$.

We note that the first two terms in (1) correspond to Wasserstein distance which improves learning performance over the Jensen-Shannon divergence used in the original GAN (Arjovsky, Chintala, and Bottou 2017; Gulrajani and

et al 2017). The third term is the gradient penalty, corresponding to the 1-Lipschitz constraint. We note that GAN based models can be difficult to train, especially in the complex time series data settings (Srivastava et al. 2017). As an example, Alaa et al. (2021) leverage a discrete Fourier transform and a spectral filter to build a time series generative model, instead of using GAN. In our work, we address this issue by introducing the last term in (1) which minimizes the squared error between the synthetic data and its true value. In such a manner, we argue that the generator attempts to generate accurate synthetic data while preserving the temporal dynamics between conditioning input and generated data by minimizing the difference between the generated data distribution P_g and real data distribution P_r .

3.2 The LSTM based Predictor

The LSTM unit (Hochreiter and Schmidhuber 1997) is composed of a cell which remembers values over arbitrary time intervals and three gates regulate the flow of information into and out of the cell. Such a design can mitigate vanishing/exploding gradients and equips LSTM with the ability of learning over long sequence of inputs. We note that transformer based models (Vaswani et al. 2017) have gained more and more popularity in language processing and time series forecasting. However, we find out that transformer based models tend to overfit more than LSTM, thus show more problem with generalizations (Zeyer et al. 2019). Therefore, we use LSTM as the core of the predictor in GenF.

3.3 The ITC Algorithm

We note that the datasets studied in this paper contain time series data for different patients, countries and sites. In the following, we refer to patients, countries, sites as units. The advantage of GenF is to balance direct and iterative forecasting so as to improve the long-range forecasting. However, the price is that we need two independent datasets: datasets \mathbb{G} and \mathbb{P} to train the CWGAN-TS synthetic data generator and the LSTM based predictor, respectively. It is possible to randomly split the entire training dataset at unit level into

Algorithm 1: The Algorithm of Generative Forecasting

Require: (i) Time series dataset $\mathbb{D} \in \mathbb{R}^{S \times M \times K}$; (ii) $\lambda, \beta=10, 15$ (see (1)); (iii) batch size = 64; (iv) Adam Optimizer (lr = 0.001).
1: Randomly split \mathbb{D} (unit level): training dataset $\mathbb{T} \in \mathbb{R}^{S_1 \times M \times K}$ (60%), i.e., $\mathbb{T} : \{X_1^i, \dots, X_M^i\}$ for $i = 1, \dots, S_1$ and $X \in \mathbb{R}^K$
test dataset $\mathbb{Q} \in \mathbb{R}^{S_2 \times M \times K}$ (20%), validation dataset $\in \mathbb{R}^{S_3 \times M \times K}$ (20%).
2: Apply the ITC algorithm to split \mathbb{T} (unit level): training dataset $\mathbb{H} \in \mathbb{R}^{S_4 \times M \times K}$ (40%), training dataset $\mathbb{P} \in \mathbb{R}^{S_5 \times M \times K}$ (60%).
3: Training dataset $\mathbb{H} \xrightarrow{\text{train}}$ the Generator (G) and Discriminator (D) in CWGAN-TS via loss function (1).
4: **for** $j = 1$ to L **do**
5: Synthetic Data Generation: $G(\mathbb{P}) = \mathbb{Y}_1 \in \mathbb{R}^{S_5 \times 1 \times K}$, i.e., $\mathbb{Y}_1 : \{\bar{X}_{M+j}^i\}$ for $i = 1, \dots, S_5$; $G(\mathbb{Q}) = \mathbb{Y}_2 \in \mathbb{R}^{S_2 \times 1 \times K}$.
6: Pruning: $\mathbb{P} \leftarrow \mathbb{P} \setminus X_j^i$, i.e., $\{X_{j+1}^i, \dots, X_{M+j-1}^i\}$ for $i = 1, \dots, S_5$; $\mathbb{Q} \leftarrow \mathbb{Q} \setminus X_j^i$.
7: Concatenation: $\mathbb{P} \leftarrow \mathbb{P} \oplus \mathbb{Y}_1$, i.e., $\{X_{j+1}^i, \dots, X_{M+j-1}^i, \bar{X}_{M+j}^i\}$ for $i = 1, \dots, S_5$; $\mathbb{Q} \leftarrow \mathbb{Q} \oplus \mathbb{Y}_2$.
8: **end for**
9: Training Dataset $\mathbb{P} \xrightarrow{\text{train}}$ LSTM based Predictor, Testing Dataset $\mathbb{Q} \xrightarrow{\text{test}}$ LSTM based Predictor.
10: **Return** MSE, MAE and sMAPE between predicted values and real values.

datasets \mathbb{G} and \mathbb{P} , but the resulting datasets may not represent the entire training dataset well. In this subsection, we address this issue by suggesting an information theoretic clustering (ITC) algorithm.

Mutual Information (MI), denoted by $I(X; Y)$, is a concrete measure from information theory (Cover and Thomas 2006) that quantifies the dependency between random variables X and Y . The ITC algorithm consists of three steps: (i) assign a score to each unit by the scoring function $J(P_i) = \sum_{P_j \in \mathbb{D}, P_j \neq P_i} I(P_i, P_j)$, where P_i refers to the candidate unit and $\mathbb{D} = \{P_1, P_2, \dots\}$ is the dataset containing all units. To estimate MI, we use a nearest neighbor based approach called KSG estimator (Kraskov, Stögbauer, and Grassberger 2004) as all features studied are continuous variables. (ii) divide all units into γ groups (of approximately equal size) based on the descending order of all scores, where γ is a tunable parameter. Therefore, units with similar scores will be grouped together and units within the same group tend to be highly dependent on each other. (iii) randomly sample from each subgroup. This is equivalent to selecting typical units of each subgroup. Random proportional sampling from all groups gives a new training dataset \mathbb{G} and the unsampled units form the new training dataset \mathbb{P} . In such a manner, we can select more typical units to better train the CWGAN-TS and the LSTM based predictor.

In summary, **the advantage of GenF over direct/iterative forecasting is two-fold:**

1. Extending the time series with synthetic data to addresses the issue of high variance forecasting due to the long prediction horizon (drawback of direct forecasting).
2. The proposed GenF attempts to address the issue of error propagation/high bias forecasting (drawback of iterative forecasting) in two ways: (i) Unlike conventional supervised learning models (e.g., transformer), the proposed CWGAN-TS combines GAN loss and MSE loss, aiming to better preserve the temporal dynamics between the generated synthetic data and the observed data. (ii) Since the synthetic data is not perfectly accurate, we only generate synthetic data for the next L time steps. Adjusting the value of L (via the validation set) is a trade-off between forecasting variance and bias. A large value of L brings GenF close to iterative forecasting, while a small value of L brings GenF close to direct forecasting.

4 Performance Evaluation

We summarize the dataset information in Section 4.1 and describe the experimental setup in Section 4.2. Next, in Section 4.3, we compare the performance of GenF to benchmark methods. Lastly, we conduct an ablation study to evaluate the effectiveness of our framework in Section 4.4.

4.1 Dataset Description

We select three public time series datasets: MIMIC-III Vital Signs dataset (Goldberger and et al 2000), Multi-Site Air Quality dataset (Zhang and et al 2017) and World Energy Consumption dataset (WorldBank 2019). The MIMIC-III Vital Signs dataset contains the first 500 patients (from subject ID 23) in the MIMIC-III Clinical database. For each patient, we extract 6 features: heart rate (bpm), respiratory rate, blood oxygen saturation (%), body temperature ($^{\circ}\text{F}$), systolic and diastolic blood pressure (mmHg). Most (over 92%) vital signs are regularly recorded at a hourly interval over a duration of 144 hours on average. The Multi-Site Air Quality dataset includes air pollutants data from 12 monitoring sites. For each site, we extract the hourly record of PM10, SO₂, NO₂, O₃, PM2.5 and CO. We note that all features are in units of ug/m^3 and each site has 35,000 records on average. The World Energy Consumption dataset contains data from 128 countries and each country contains three annual energy consumption indicators: electricity (kWh per capita), fossil fuel (% of total) and renewable energy (% of total) from 1971 to 2014. For each dataset, a small amount (i.e., less than 5%) of missing values are imputed using the last historical readings. Moreover, we scale all variables to $[0, 1]$ and reshape all scaled data via a sliding observation window into a three dimensional dataset $\mathbb{D} \in \mathbb{R}^{S \times M \times K}$.

4.2 Experiment Setup

In the experiment, the dataset \mathbb{D} is randomly split into three subsets at unit level: training dataset $\mathbb{T} \in \mathbb{R}^{S_1 \times M \times K}$ (60%), test dataset $\mathbb{Q} \in \mathbb{R}^{S_2 \times M \times K}$ (20%) and validation dataset $\in \mathbb{R}^{S_3 \times M \times K}$ (20%). We note that both GenF and the benchmark methods are trained using the training dataset \mathbb{T} , and the test dataset \mathbb{Q} is used to evaluate the performance. **To ensure fair comparison, we conduct grid search over all tunable hyper-parameters and possible configurations using the validation dataset.** We highlight that all methods

Generative Forecasting (GenF)		
CWGAN-TS		Predictor
Generator	Discriminator	-
$(S, M + 1, K)$	$(S, M + 1, K)$	(S, M, K)
LSTM (5)	LSTM (5)	LSTM (5)
Linear (12)	Linear (12)	LSTM (5)
Linear (K)	Linear (4)	Linear (4)
Reshape $(S, 1, K)$	Linear (1)	Linear (1)

LSTNet
skip-length $p = 5$, gradient clipping = 10, epoch = 1000, dropout = 0.1, batchsize = 64.
TLSTM
learning rate (lr) decay = 0.8, lr = $1e-3$, dropout = 0.1, batchsize = 64, epoch = 1000.
LogSparse
embedding size = 16, kernel size = 9 batchsize = 64, epoch = 1000, lr = $3e-3$.

Table 1: (left) Network configuration of Generative Forecasting (GenF). The fourth row represents the shape of input variables and the parameter in Linear(\cdot) is the number of output units in the linear layer. The parameter in LSTM(\cdot) is the hidden state size. (right) Key parameters of the three strong baselines.

share the same grid search range and step size. Specifically, some key parameters are tuned as follows. (i) for all LSTM based networks (including GenF), the hidden state size of LSTM is tuned from 5 to 100 with step size of 5 and number of LSTM layers and fully connected layers are tuned from 1 to 10 with step size of 1. (ii) for SVR, the regularization coefficient c is chosen from $\{0.01, 0.1, 1, 10, 50\}$. (iii) for GPR, the noise level α is chosen from $\{1^{-10}, 1^{-8}, \dots, 1, 10\}$.

We now provide a list of tuned parameters for predicting systolic blood pressure using the MIMIC-III Vital Signs dataset. In terms of the four classical models used to implement iterative forecasting and direct forecasting, (i) SVR (kernel = rbf) and (ii) GPR (kernel = rbf) are trained using the flatted training dataset \mathbb{T} . (iii) ARIMA (2,0,1) is trained using the past M historical values of a single feature (e.g., systolic blood pressure). (iv) for LSTM, we stack two LSTM layers (each LSTM with hidden size of 10) and two fully connected layers (with size of 10 and 1, respectively). This LSTM based neural network is directly trained using training dataset \mathbb{T} for 1000 epochs using Adam (Kingma and Ba 2014) with a learning rate of 0.001, in batches of 64. As for the three strong baselines (TLSTM, LSTNet, LogSparse), we refer to the source code released by their authors and some key parameters for those baselines are summarized in Table 1 (right). In terms of GenF, the training and testing procedures are summarized in Algorithm 1. We note

that both the CWGAN-TS and the LSTM based predictor in GenF are trained using Adam (Kingma and Ba 2014) with a learning rate of 0.001, in batches of 64 and sigmoid activation (Goodfellow, Bengio, and Courville 2016). **We use NVIDIA RTX 2080 Ti devices for our experiments and the source code (including random seeds) will be released for reproducibility (see Supplementary Material).**

In the experiments, we compare the performance of GenF to direct/iterative forecasting and the three strong baselines. The Mean Squared Error (MSE) and Mean Absolute Error (MAE) are used to evaluate the performance, where the former captures both the variance and the bias of the predictor, and the latter is useful for understanding whether the size of the error is of concern or not. Furthermore, a scale invariant error metric called symmetric Mean Absolute Percentage Error (sMAPE) (Hyndman and Koehler 2006) is also used. In Table 2, we show the performance of three variants of GenF, namely GenF-1, GenF-2, GenF-3, where the 'X' in GenF-X represents the value of the synthetic window length L . We only show the performance up to $L = 3$ as a larger value of L cannot outperform GenF-3 from $t + 1$ to $t + 8$. Lastly, the forecasting performance for the time steps that are part of the generator are not shown. For example, GenF-1 generates synthetic data for time step $(t + 1)$ and makes predictions for subsequent time steps $(t + 2, \dots)$. Hence, the forecasting performance at $t + 1$ is not shown.

Prediction Horizon		$t + 1$	$t + 2$	$t + 3$	$t + 4$	$t + 6$	$t + 8$
Direct	LSTM	85.3 ± 3.0	106 ± 6.8	121 ± 6.5	127 ± 6.4	146 ± 7.7	153 ± 9.3
	SVR	97.2 ± 5.4	126 ± 9.8	136 ± 11	151 ± 13	158 ± 13	173 ± 18
	GPR	105 ± 4.2	115 ± 5.2	131 ± 9.2	150 ± 11	165 ± 12	169 ± 13
Iterative	LSTM	85.3 ± 2.0	104 ± 4.3	127 ± 5.1	135 ± 6.0	159 ± 6.1	161 ± 5.8
	SVR	97.2 ± 5.4	114 ± 9.2	140 ± 11	167 ± 12	177 ± 13	197 ± 14
	GPR	105 ± 4.2	119 ± 4.8	129 ± 6.1	135 ± 9.1	161 ± 11	177 ± 12
	ARIMA	119 ± 5.3	136 ± 6.8	134 ± 7.4	156 ± 6.6	200 ± 8.3	214 ± 13
LogSparse		91.5 ± 3.5	103 ± 4.2	111 ± 5.0	115 ± 6.5	121 ± 8.7	149 ± 7.3
TLSTM		89.5 ± 4.0	105 ± 5.5	109 ± 6.1	117 ± 4.0	131 ± 9.1	148 ± 7.8
LSTNet		83.5 ± 3.1	102 ± 3.5	115 ± 4.1	120 ± 7.0	133 ± 7.1	153 ± 6.8
GenF-1		-	99 ± 7.0	110 ± 9.3	114 ± 5.8	126 ± 7.3	144 ± 10.9
GenF-2		-	-	103 ± 9.2	108 ± 9.9	121 ± 9.0	141 ± 9.5
GenF-3		-	-	-	101 ± 10	114 ± 8.4	133 ± 11

Table 2: Performance (MSE \pm standard deviation) of predicting systolic blood pressure using three variants of GenF, iterative/direct forecasting and three strong baselines using the MIMIC-III Vital Signs dataset. Similar performance trends can be observed using the Multi-Site Air Quality dataset (forecasting NO₂ emission), the World Energy Consumption dataset (forecasting fossil fuel consumption) and MIMIC-III Vital Signs dataset (forecasting heart rate) (see Fig. 4 in the **Appendix**).

Prediction Horizon	$t + 8$		$t + 12$		$t + 30$		$t + 60$	
	MAE	sMAPE	MAE	sMAPE	MAE	sMAPE	MAE	sMAPE
LogSparse	6.6 ± 0.7	$5.5 \pm 0.3\%$	8.1 ± 0.5	$6.9 \pm 0.6\%$	11.6 ± 1.0	$9.7 \pm 0.9\%$	14.5 ± 2.8	$11.3 \pm 1.2\%$
TLSTM	6.8 ± 0.4	$5.7 \pm 0.4\%$	8.2 ± 0.6	$7.1 \pm 0.8\%$	12.3 ± 1.2	$10.9 \pm 1.1\%$	15.0 ± 2.3	$12.7 \pm 1.5\%$
LSTNet	6.9 ± 0.6	$5.8 \pm 0.4\%$	8.2 ± 0.7	$7.0 \pm 0.7\%$	12.0 ± 1.3	$10.6 \pm 1.3\%$	14.2 ± 2.6	$11.5 \pm 0.9\%$
GenF-3	6.2 ± 0.5	$5.1 \pm 0.4\%$	7.5 ± 0.7	$6.3 \pm 0.5\%$	10.9 ± 1.4	$9.0 \pm 0.9\%$	13.7 ± 2.9	$10.9 \pm 1.8\%$
GenF-6	6.4 ± 0.3	$5.2 \pm 0.2\%$	7.4 ± 0.5	$6.3 \pm 0.4\%$	10.5 ± 1.1	$8.7 \pm 0.8\%$	12.4 ± 2.7	$10.3 \pm 1.6\%$
Min. Improvement	6.06%	7.27%	8.64%	8.70%	9.48%	10.3%	12.67%	8.85%

Table 3: Performance (MAE, sMAPE \pm standard deviation) of predicting systolic blood pressure using MIMIC-III for GenF and strong baselines. Similar performance trends can be observed using two other datasets (see Tables 4 and 5 in the **Appendix**).

4.3 Performance Comparison

Performance of Classical Approaches: In Table 2 (rows 1 - 7), we compare the performance of GenF to iterative/direct forecasting implemented by the four classical models. We find that the iterative/direct forecasting implemented by LSTM generally outperforms other implementations (e.g., GPR and SVR). This finding agrees with the result stated in (Ma et al. 2015; Lipton et al. 2015; Malhotra et al. 2015). For other models, ARIMA tends to perform worse as it uses only a single feature which may not benefit from the interaction among multiple features. Some papers (Contreras et al. 2003) also point out that ARIMA is poor at predicting turning points as it is essentially ‘backward looking’. Moreover, we note that the performance of direct and iterative forecasting implemented by ARIMA are the same due to its recursive nature. Lastly, the performance of kernel based methods (GPR and SVR) generally lies in between LSTM and ARIMA. We posit this is because the time series data can be non-stationary and the optimal kernel function may change over time (Wilson and Adams 2013; Wilson et al. 2016).

Performance of GenF vs Strong Baselines: In Table 2 (rows 8 - 10), we compare the performance of GenF to the three strong baselines. We find that the performance of the strong baselines generally can outperform iterative/direct forecasting implemented by the four classical models. Comparing to GenF, we find that the performance of GenF-3 is better than the strong baselines. For example, the MSE of the best performing benchmark, LogSparse, at $t+4$ is 115 while the MSE of GenF-3 at $t+4$ is 101, which is approximately 12.2% lower. Similar or greater improvements can be observed using the the Multi-Site Air Quality dataset and the World Energy Consumption dataset as well (see Fig. 4 in the **Appendix**). Lastly, we have discussed with domain experts on the relevance of our long-range forecasting results (e.g., at $t+4$) of the blood pressure. The feedback from clinicians is that the MSE performance is acceptable for interventional purposes for ICU patients and at-home high risk patients.

Longer Prediction Horizons Using MAE and sMAPE: We now explore much longer prediction horizons of up to $t+60$ and summarize the performance of predicting systolic blood pressure using MAE and sMAPE in Table 3. We can see that the performance of GenF-3 outperforms the best performing baseline (i.e., LogSparse) by 6.06% at $t+8$. As the prediction horizon grows, GenF-6 tends to obtain the best performance, resulting in an improvement (in MAE) of 9.48% at $t+30$ and 12.67% at $t+60$. Interestingly, gen-

erating more synthetic data (e.g., GenF-10) cannot perform GenF-6 at $t+12$, $t+30$ and $t+60$. It suggests that for longer prediction horizon, we should shift GenF more towards iterative forecasting by slightly increasing L , but not too much. Similar performance trends can be observed using the other two datasets (see Tables 4 and 5 in the **Appendix**).

Complexity Comparison: We now compare the model complexity of GenF to the three strong baselines when predicting the systolic blood pressure. The parameter count for each model is summarized as follows: (i) GenF: 5.3K (3K for CWGAN-TS and 2.3K for Predictor), (ii) TLSTM: 8.4K, (iii) LSTNet: 19.2K and (iv) LogSparse: 37.1K. It can be seen that the parameters of GenF are at least 37% (compare GenF to TLSTM) less than strong baselines, facilitating the use of GenF in resource-constrained devices.

4.4 Ablation Study

To demonstrate the effectiveness of key components in GenF, we conduct an ablation study. Specifically, we remove one component at a time in GenF and observe the impact on synthetic data generation and forecasting performance. We construct several variants of CWGAN-TS as follows.

- **CWGAN-GP:** CWGAN-TS without the squared error penalty term in the loss function (1).
- **CWGAN-RS:** CWGAN-TS without the ITC algorithm, instead, the CWGAN-TS is trained with a randomly selected subset of the training dataset T .
- **GAN:** A conventional GAN (Goodfellow and et al 2014) without considering the Wasserstein distance.

Experiment Setup: In the experiment of predicting heart rate, we shortlist a unit called Subject ID 23 and show the observation window ($M = 20$), synthetic window ($L = 3$) and the prediction horizon in Fig. 3. Specifically, in the synthetic window, we show the synthetic data recursively generated by CWGAN-TS, its three variants and the four classical models (SVR, GPR, ARIMA and LSTM) up to $t = 23$. In the prediction horizon, we use the same LSTM based predictor as before (trained on the training dataset) to evaluate the forecasting performance of all models by using their past observations and the synthetic data ($t = 21$ to 23). As a comparison, we also show the true value (solid line). In Fig. 3, the values in parentheses are the MSE of the synthetic data generation and the forecasting performance, averaged over the synthetic window and prediction horizon, respectively.

Synthetic Data Generation: Fig. 3 shows the synthetic data generation performance of various methods (see left

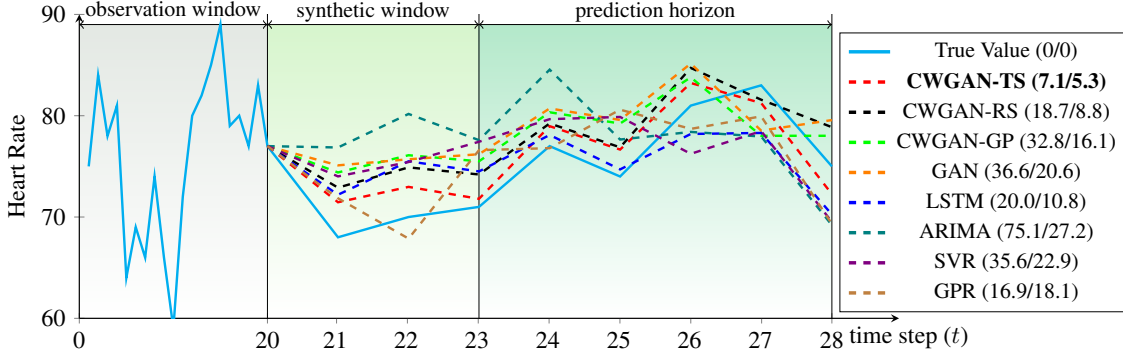


Figure 3: Synthetic data recursively generated by various models and their corresponding forecasting performance based on observed and generated data, for predicting heart rate using the MIMIC-III Vital Signs dataset (Subject ID 23). The values in parentheses are the MSE of the synthetic data generation and the forecasting performance, averaged over the synthetic window and prediction horizon, respectively. See Fig. 5 in the **Appendix** for results on other subjects.

number in parentheses). For the four classical models (SVR, GPR, ARIMA and LSTM), LSTM has the smallest MSE. Comparing CWGAN-TS to LSTM, we find that both of them can capture the rising trend of heart rate, but the synthetic data generated by CWGAN-TS is more stable and accurate. Specifically, the performance of LSTM and CWGAN-TS at $t = 21$ (the first synthetic data) are comparable. Subsequently, the synthetic data generated by LSTM tends to fluctuate greatly, resulting in a larger MSE. We posit this is caused by error propagation. As for CWGAN-TS, we see that CWGAN-TS is essentially a combination of LSTMs (see Table 1(left)), with the key difference being that CWGAN-TS incorporates an additional GAN loss, but results in more stable synthetic data with a 65% lower MSE than LSTM. This demonstrates the effectiveness of the GAN loss in mitigating error propagation and similar stabilized effect can also be observed in (Zhu et al. 2017; Frid-Adar et al. 2018a). Interestingly, the LSTM has 3.5K parameters while CWGAN-TS has only 3K parameters.

When comparing CWGAN-TS to CWGAN-GP, we find that the squared error penalty term in (1) significantly improves performance (i.e., 78%), suggesting the crucial role of the error penalty term. Moreover, when comparing CWGAN-TS to CWGAN-RS, the results show that the ITC algorithm improves forecasting performance by 62%, indicating its effectiveness in selecting typical units. Comparing to the original GAN, CWGAN-TS improves performance by 81% in generating synthetic data. We posit this is because CWGAN-TS uses Wasserstein distance as part of the loss function, leading to a more stable learning process.

Forecasting Performance: Fig. 3 also shows the forecasting performance for the various methods (see right number in parentheses). We observe that CWGAN-TS has approximately 40%, 51%, 67%, and 74% improvement over CWGAN-RS, LSTM, CWGAN-GP, and GAN, respectively. As expected, the model that generates more accurate synthetic data tends to have better forecasting performance, suggesting the important role of the CWGAN-TS and the ITC algorithm in improving long-range forecasting. Lastly, we note that similar performance trends can be observed for other subjects as well (see Fig. 5 in the **Appendix**).

5 Reflections

GenF is a competitive long-range forecasting strategy that uses GAN-based synthetic data to strike a balance between iterative and direct forecasting. We conclude by discussing some relevant points and avenues for future research.

Averaged Performance over All Subjects: The performance in Section 4.4 on *individual subjects* demonstrates the effectiveness of CWGAN-TS. We also study the performance *averaged over all subjects*. In addition to the four classical models and the three strong baselines, we also explore a state-of-the-art GAN based model called TimeGAN (Yoon, Jarrett, and van der Schaar 2019) to generate synthetic data. We summarize the average performance of synthetic data generation and long-range forecasting in Table 6 in the **Appendix**, where we observe that CWGAN-TS outperforms the best performing benchmark by up to 10% in synthetic data generation and long-range forecasting.

Selection of the Synthetic Window Length L : The forecasting performance of GenF depends on the choice of L . Our results suggest that as the prediction horizon grows, we should increase the value of L (i.e., $L = 3$ for $t + 10$, $L = 6$ for $t + 12$, $t + 30$ and $t + 60$ in Table 3). We suggest using L as a hyper-parameter and tuning it via the validation dataset, but a theoretical approach to determine L is worth exploring.

The ITC Algorithm: In the ITC algorithm, we only use first order mutual information as the scoring function. We note that other types of scoring functions, such as joint mutual information, conditional mutual information or pairwise mutual information, could be a better choice for the scoring function. We will explore them in our future research.

PICV and TSCV: We note that our cross validation (CV) method of doing random train-test split at the unit level is known as Population-Informed CV (PICV). PICV is more practical as it requires no prior knowledge about the unseen data. We understand that PICV may cause data leakage as there may be correlations across different units. Therefore, we also examine Time Series CV (TSCV) which splits the data in chronological order. Our experimental results on the Multi-Site Air Quality dataset demonstrate that by using TSCV, the proposed GenF outperforms the strong baselines by at least 7.8% (see Table 7 in the **Appendix**).

References

- Ahmed, N.; Atiya, A.; and Gayar, N. 2007. A Combined Neural Network/Gaussian Process Regression Time Series Forecasting System for the NN3 Competition.
- Al-Saba, T.; and El-Amin, I. 1999. Artificial neural networks as applied to long-term demand forecasting. *Artificial Intelligence in Engineering*, 13(2): 189–197.
- Alaa, A.; et al. 2021. Generative Time-series Modeling with Fourier Flows. In *International Conference on Learning Representations (ICLR)*.
- Alvarez, F. M.; et al. 2010. Energy time series forecasting based on pattern sequence similarity. *IEEE Transactions on Knowledge and Data Engineering*, 23(8): 1230–1243.
- Arjovsky, M.; Chintala, S.; and Bottou, L. 2017. Wasserstein Generative Adversarial Networks. In *International Conference on Machine Learning (ICML)*, volume 70, 214–223.
- Azad, H. B.; Mekhilef, S.; and Ganapathy, V. G. 2014. Long-term wind speed forecasting and general pattern recognition using neural networks. *IEEE Transactions on Sustainable Energy*, 5(2): 546–553.
- Bica, I.; et al. 2020. Estimating counterfactual treatment outcomes over time through adversarially balanced representations. *arXiv preprint arXiv:2002.04083*.
- Bontempi, G. 2008. Long term time series prediction with multi-input multi-output local learning. *Proc. 2nd ESTSP*, 145–154.
- Bontempi, G.; and Taieb, S. B. 2011. Conditionally dependent strategies for multiple-step-ahead prediction in local learning. *International journal of forecasting*, 27(3): 689–699.
- Bontempi, G.; Taieb, S. B.; and Le Borgne, Y.-A. 2012. Machine learning strategies for time series forecasting. In *European Business Intelligence Summer School*, 62–77. Springer.
- Bowles, C.; et al. 2018. GAN augmentation: Augmenting training data using generative adversarial networks. *arXiv preprint arXiv:1810.10863*.
- Box, G. E. P.; and Pierce, D. A. 1970. Distribution of residual autocorrelations in autoregressive-integrated moving average time series models. *Journal of the American Statistical Association*, 65(332): 1509–1526.
- Cheng, J.; Huang, K.; and Zheng, Z. 2020. Towards Better Forecasting by Fusing Near and Distant Future Visions. In *AAAI Conference on Artificial Intelligence*, 3593–3600.
- Choi, E.; and et al. 2016. Using recurrent neural network models for early detection of heart failure onset. *Journal of the American Medical Informatics Association*, 24(2): 361–370.
- Contreras, J.; et al. 2003. ARIMA models to predict next-day electricity prices. *IEEE Transactions on Power Systems*, 18(3): 1014–1020.
- Cortes, C.; and Vapnik, V. 1995. Support-vector networks. *Machine learning*, 20(3): 273–297.
- Cover, T. M.; and Thomas, J. A. 2006. *Elements of Information Theory, 2nd edition*. John Wiley & Sons.
- Dong, H.-W.; et al. 2018. Musegan: Multi-track sequential generative adversarial networks for symbolic music generation and accompaniment. In *AAAI Conference on Artificial Intelligence*.
- Esteban, C.; Hyland, S. L.; and Rätsch, G. 2017. Real-valued (medical) time series generation with recurrent conditional GANs. *arXiv preprint arXiv:1706.02633*.
- Frid-Adar, M.; et al. 2018a. GAN-based synthetic medical image augmentation for increased CNN performance in liver lesion classification. *Neurocomputing*, 321: 321–331.
- Frid-Adar, M.; et al. 2018b. Synthetic data augmentation using GAN for improved liver lesion classification. In *IEEE International Symposium on Biomedical Imaging*, 289–293. IEEE.
- Goldberger, A. L.; and et al. 2000. PhysioToolkit, and PhysioNet: Components of a New Research Resource for Complex Physiologic Signals. *Circulation*, 101(23): e215 – e220.
- Goodfellow, I.; Bengio, Y.; and Courville, A. 2016. *Deep learning*. MIT press.
- Goodfellow, I.; and et al. 2014. Generative adversarial nets. In *Advances in Neural Information Processing Systems (Neurips)*, 2672–2680.
- Granger, C. W. J.; and Newbold, P. 2014. *Forecasting economic time series*. Academic Press.
- Guen, V. L.; and Thome, N. 2019. Shape and time distortion loss for training deep time series forecasting models. In *Advances in Neural Information Processing Systems (Neurips)*.
- Gulrajani, I.; and et al. 2017. Improved training of wasserstein gans. In *Advances in Neural Information Processing Systems (Neurips)*, 5767–5777.
- Haidar, M. A.; and Rezagholizadeh, M. 2019. Textkd-GAN: Text generation using knowledge distillation and generative adversarial networks. In *Canadian Conference on Artificial Intelligence*, 107–118. Springer.
- Hamzaçebi, C.; Akay, D.; and Kutay, F. 2009. Comparison of direct and iterative artificial neural network forecast approaches in multi-periodic time series forecasting. *Expert Systems with Applications*, 36(2): 3839–3844.
- Hochreiter, S.; and Schmidhuber, J. 1997. Long short-term memory. *Neural computation*, 9(8): 1735–1780.
- Hyndman, R. J.; and Koehler, A. B. 2006. Another look at measures of forecast accuracy. *International journal of forecasting*, 22(4): 679–688.
- Jarrett, D.; et al. 2021. Clairvoyance: A Pipeline Toolkit for Medical Time Series. In *International Conference on Learning Representations (ICLR)*.
- Kingma, D. P.; and Ba, J. 2014. Adam: A method for stochastic optimization. *arXiv preprint arXiv:1412.6980*.
- Kraskov, A.; Stögbauer, H.; and Grassberger, P. 2004. Estimating mutual information. *Physical Review E*, 69(6): 066–138.
- Lai, G.; et al. 2018. Modeling long-and short-term temporal patterns with deep neural networks. In *The 41st International ACM SIGIR Conference on Research & Development in Information Retrieval*, 95–104.

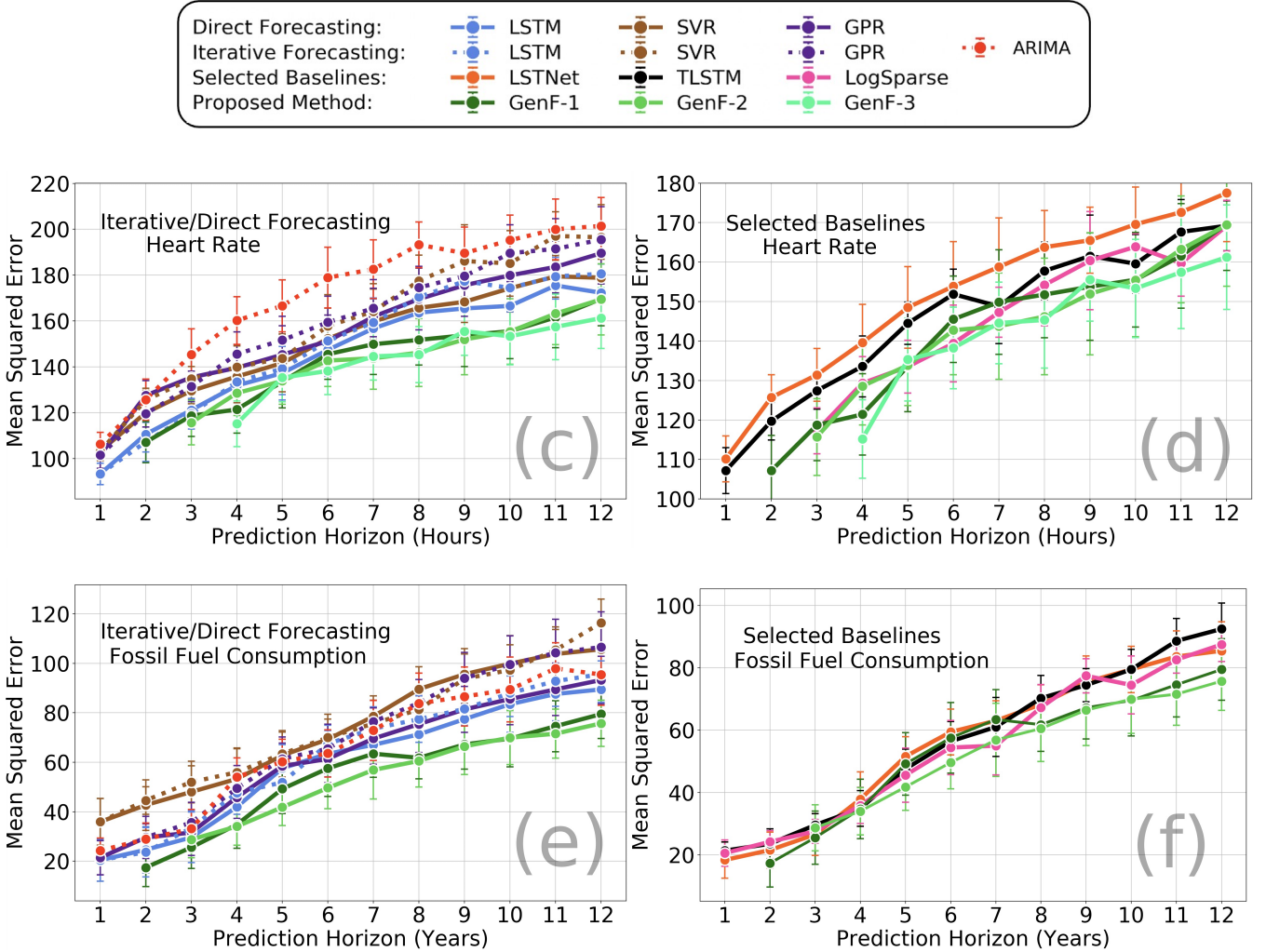
- Li, S.; et al. 2019. Enhancing the locality and breaking the memory bottleneck of transformer on time series forecasting. In *International Conference on Neural Information Processing Systems (Neurips)*.
- Lipton, Z. C.; et al. 2015. Learning to diagnose with LSTM recurrent neural networks. *arXiv preprint arXiv:1511.03677*.
- Ma, X.; et al. 2015. Long short-term memory neural network for traffic speed prediction using remote microwave sensor data. *Transportation Research Part C: Emerging Technologies*, 54: 187–197.
- Malhotra, P.; et al. 2015. Long short term memory networks for anomaly detection in time series. In *23rd European Symposium on Artificial Neural Networks, Computational Intelligence and Machine Learning*.
- Marcellino, M.; Stock, J. H.; and Watson, M. W. 2006. A comparison of direct and iterated multistep AR methods for forecasting macroeconomic time series. *Journal of econometrics*, 135(1-2): 499–526.
- Mirza, M.; and Osindero, S. 2014. Conditional generative adversarial nets. *arXiv preprint arXiv:1411.1784*.
- Mogren, O. 2016. C-RNN-GAN: Continuous recurrent neural networks with adversarial training. *arXiv preprint arXiv:1611.09904*.
- Nguyen, H. H.; and Chan, C. W. 2004. Multiple neural networks for a long term time series forecast. *Neural Computing & Applications*, 13(1): 90–98.
- Rangapuram, S. S.; et al. 2018. Deep state space models for time series forecasting. *Advances in Neural Information Processing Systems (Neurips)*, 31: 7785–7794.
- Rasmussen, C. E. 2003. Gaussian processes in machine learning. In *Summer School on Machine Learning*, 63–71. Springer.
- Sen, R.; Yu, H.-F.; and Dhillon, I. 2019. Think globally, act locally: A deep neural network approach to high-dimensional time series forecasting. *Advances in Neural Information Processing Systems (Neurips)*.
- Shin, H.-C.; et al. 2018. Medical image synthesis for data augmentation and anonymization using generative adversarial networks. In *International Workshop on Simulation and Synthesis in Medical Imaging*, 1–11. Springer.
- Sorjamaa, A.; and et al. 2007. Methodology for long-term prediction of time series. *Neurocomputing*, 70(16-18): 2861–2869.
- Srivastava, A.; et al. 2017. Veegan: Reducing mode collapse in gans using implicit variational learning. *Advances in Neural Information Processing Systems (Neurips)*.
- Sutskever, I.; Vinyals, O.; and Le, Q. V. 2014. Sequence to sequence learning with neural networks. In *Advances in Neural Information Processing Systems (Neurips)*, 3104–3112.
- Taieb, S. B.; et al. 2012. A review and comparison of strategies for multi-step ahead time series forecasting based on the NN5 forecasting competition. *Expert systems with applications*, 39(8): 7067–7083.
- Vaswani, A.; et al. 2017. Attention is all you need. In *Advances in neural information processing systems*, 5998–6008.
- Weigend, A. S.; and Gershenfeld, N. A. 2018. *Time series prediction: forecasting the future and understanding the past*. Routledge.
- Wilson, A.; and Adams, R. 2013. Gaussian process kernels for pattern discovery and extrapolation. In *International Conference on Machine Learning (ICML)*, 1067–1075.
- Wilson, A. G.; et al. 2016. Deep kernel learning. In *Artificial Intelligence and Statistics*, 370–378.
- WorldBank. 2019. Electricity & Fossil Fuel Energy Consumption. *World Development Indicator*.
- Yoon, J.; Jarrett, D.; and van der Schaar, M. 2019. Time-series generative adversarial networks. In *Advances in Neural Information Processing Systems (Neurips)*, 5508–5518.
- Yu, R.; et al. 2017. Long-term forecasting using tensor-train rnns. *Arxiv, ArXiv Preprint:1711.00073*.
- Zeyer, A.; et al. 2019. A Comparison of Transformer and LSTM Encoder Decoder Models for ASR. In *2019 IEEE Automatic Speech Recognition and Understanding Workshop (ASRU)*, 8–15.
- Zhang, S.; and et al. 2017. Cautionary tales on air-quality improvement in Beijing. In *Proceedings of the Royal Society A: Mathematical, Physical and Engineering Sciences*, 473(2205).
- Zhu, J.-Y.; et al. 2017. Toward multimodal image-to-image translation. In *Advances in Neural Information Processing Systems (Neurips)*, 465–476.

A Supplementary Results

In this Appendix, we first present the performance comparison (MSE) on the MIMIC-III Vital Signs dataset with another forecasting target (i.e., heart rate), Multi-Site Air Quality dataset (forecasting NO₂ emissions) and the World Energy Consumption dataset (forecasting fossil fuel consumption) in Section A.1. Furthermore, the performance comparison (MAE, sMAPE) for longer horizons are provided in Section A.2. Next, we conduct an ablation study on more subjects and provide the experimental results in Section A.3. Moreover, we also show the averaged performance of all subjects in the ablation study in Section A.4. Lastly, we evaluate the performance of GenF using Time Series Cross Validation (TSCV) and compare it to the performance of Population-Informed Cross Validation (PICV) in Section A.5.

A.1 Performance Comparison on More Datasets

We repeat our experiments in Section 4.2 using the MIMIC-III Vital Signs dataset with another forecasting target (i.e., heart rate), Multi-Site Air Quality dataset (forecasting NO₂ emissions) and the World Energy Consumption dataset (forecasting fossil fuel consumption). We follow the same parameter tuning procedure in Section 4.2 and present the results in Fig. 4. We can see the results largely mirror those in Table 2 : the proposed GenF has better forecasting performance than the classical approaches and the three strong baselines. For example, in Fig. 4 (h), the MSE of LSTNet at $t + 3$ is 427 while the MSE of GenF-3 at $t + 4$ is 360, which is approximately 16% lower.



A.2 More Results for Longer Prediction Horizons Using MAE

We now present the performance comparison between the proposed GenF and three strong baselines for longer prediction horizons using MAE and sMAPE. The performance comparisons using the World Energy Consumption Quality dataset and

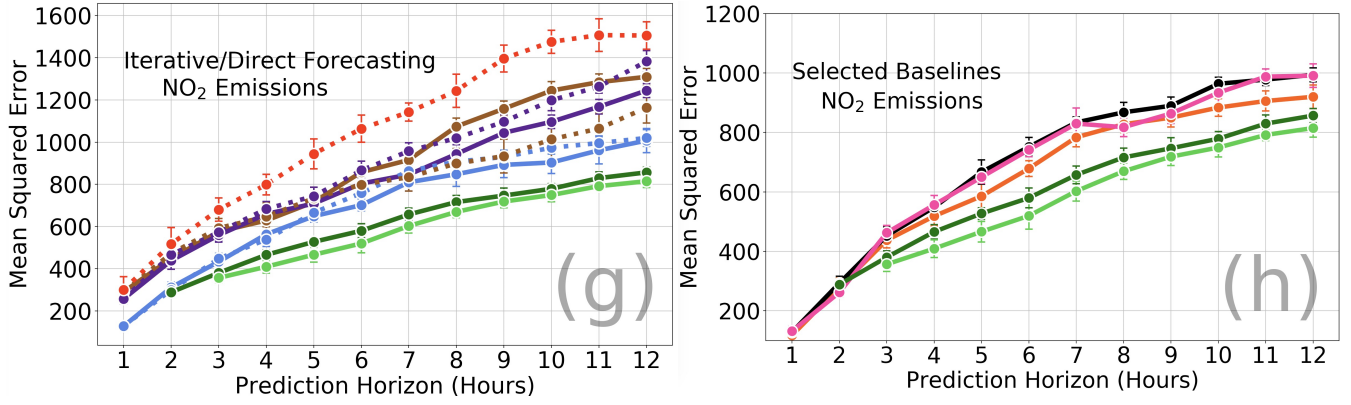


Figure 4: Performance comparison between three variants of GenF (GenF-1, GenF-2, GenF-3) and iterative/direct forecasting ((c), (e), (g)), three strong baselines ((d), (f), (h)) using the MIMIC-III Vital Signs dataset with another forecasting target (i.e., heart rate) (upper row), World Energy Consumption Quality dataset (middle row) and the Multi-Site Air Quality dataset (lower row). In each subfigure, we highlight the prediction target and the method used. Each plot is averaged over 10 runs and the error-bar is the standard derivation. The performance of GenF in the left and right columns looks different due to the different scales, but the values are the same.

the Multi-Site Air Quality dataset are summarized in Tables 4 and 5, respectively. We can see that the predictive performance largely mirror those in Table 3: the improvement of the proposed GenF over the three strong baselines tends to increase as the prediction horizon grows (i.e., 8.16% - 14.4% in Table 4 and 8.42% - 13.6% in Table 5).

Prediction Horizon	t + 8		t + 12		t + 15		t + 18	
	MAE	sMAPE	MAE	sMAPE	MAE	sMAPE	MAE	sMAPE
LogSparse	4.1 ± 0.3	4.7±0.5 %	4.9 ± 0.3	6.1±0.4 %	6.6 ± 0.2	8.2±0.9 %	7.6 ± 0.2	9.8±1.5 %
TLSTM	4.2 ± 0.2	5.0±0.3 %	5.7 ± 0.1	7.3±0.5 %	6.9 ± 0.3	8.9±1.1 %	8.2 ± 0.3	10.8±1.7 %
LSTNet	4.0 ± 0.1	4.7±0.4 %	5.2 ± 0.2	6.2±0.8 %	6.8 ± 0.3	8.7±0.8 %	7.9 ± 0.3	10.5±1.3 %
GenF-2	3.6 ± 0.2	4.4±0.6 %	4.6 ± 0.2	5.5±0.7 %	6.1 ± 0.2	7.8±1.2 %	7.1 ± 0.5	8.9±1.1 %
GenF-3	3.6 ± 0.2	4.5±0.4 %	4.5 ± 0.3	5.4±0.6 %	5.9 ± 0.3	7.6±1.0 %	6.8 ± 0.4	8.5±0.8 %
GenF-5	3.7 ± 0.2	4.5±0.5 %	4.6 ± 0.4	5.5±0.4 %	5.8 ± 0.3	7.5±0.9 %	6.5 ± 0.3	8.4±0.7 %
Min Improvement	10%	6.4%	8.16%	11.5%	12.1%	8.54%	14.4%	14.2%

Table 4: Performance comparison (MAE, sMAPE ± standard deviation) between three variants of GenF and three strong baselines in fossil fuel consumption using the World Energy Consumption dataset. Due to the time span of the dataset (from 1971 to 2014), we only show predictive performance up to t + 18.

Prediction Horizon	t + 8		t + 12		t + 30		t + 60	
	MAE	sMAPE	MAE	sMAPE	MAE	sMAPE	MAE	sMAPE
LogSparse	18.1 ± 1.5	20 ± 4 %	21.5 ± 1.5	24 ± 6 %	23.5 ± 2.3	26 ± 5 %	26.7 ± 2.6	29 ± 8 %
TLSTM	18.8 ± 1.0	20 ± 5 %	20.7 ± 1.9	22 ± 8 %	24.0 ± 2.0	28 ± 9 %	27.5 ± 2.3	31 ± 9 %
LSTNet	17.8 ± 2.0	18 ± 3 %	19.9 ± 1.8	21 ± 9 %	23.6 ± 2.2	25 ± 6 %	27.0 ± 2.5	28 ± 10 %
GenF-2	16.3 ± 1.8	16 ± 3 %	18.0 ± 1.7	19 ± 6 %	20.5 ± 2.2	23 ± 9 %	24.2 ± 2.5	27 ± 12 %
GenF-3	16.5 ± 1.8	16 ± 5 %	18.2 ± 2.0	19 ± 4 %	20.3 ± 2.4	23 ± 8 %	24.0 ± 2.4	26 ± 9 %
GenF-6	16.9 ± 1.3	17 ± 3 %	18.5 ± 1.9	19 ± 3 %	19.7 ± 2.0	22 ± 5 %	22.9 ± 1.8	25 ± 8 %
Min Improvement	8.42%	11.1%	9.54%	9.52%	13.6%	12%	10.1%	10.7%

Table 5: Performance comparison (MAE, sMAPE ± standard deviation) between three variants of GenF and three strong baselines in predicting NO₂ emission using the Multi-Site Air Quality dataset.

A.3 Ablation Study on More Units

We repeat our ablation study using Subjects ID 109 and 890 in the MIMIC-III Vital Sign dataset. In Fig. 5, we observe that the proposed CWGAN-TS can generate more accurate and stable synthetic data as compared to other studied approaches. The error penalty term and the ITC algorithm can help to improve the performance in generating synthetic data. For example, in the upper figure, when comparing CWGAN-TS to CWGAN-RS, the results demonstrate that the ITC algorithm helps to improve the performance by 34%, indicating its effectiveness in selecting typical units. Compared to the CWGAN-GP, CWGAN-TS improves performance by 80% in generating synthetic data, suggesting the crucial role of the error penalty term. Furthermore, the model that can generate accurate synthetic data tends to have better forecasting performance. This suggests the important role of the CWGAN-TS and the ITC algorithm in improving long-range forecasting.

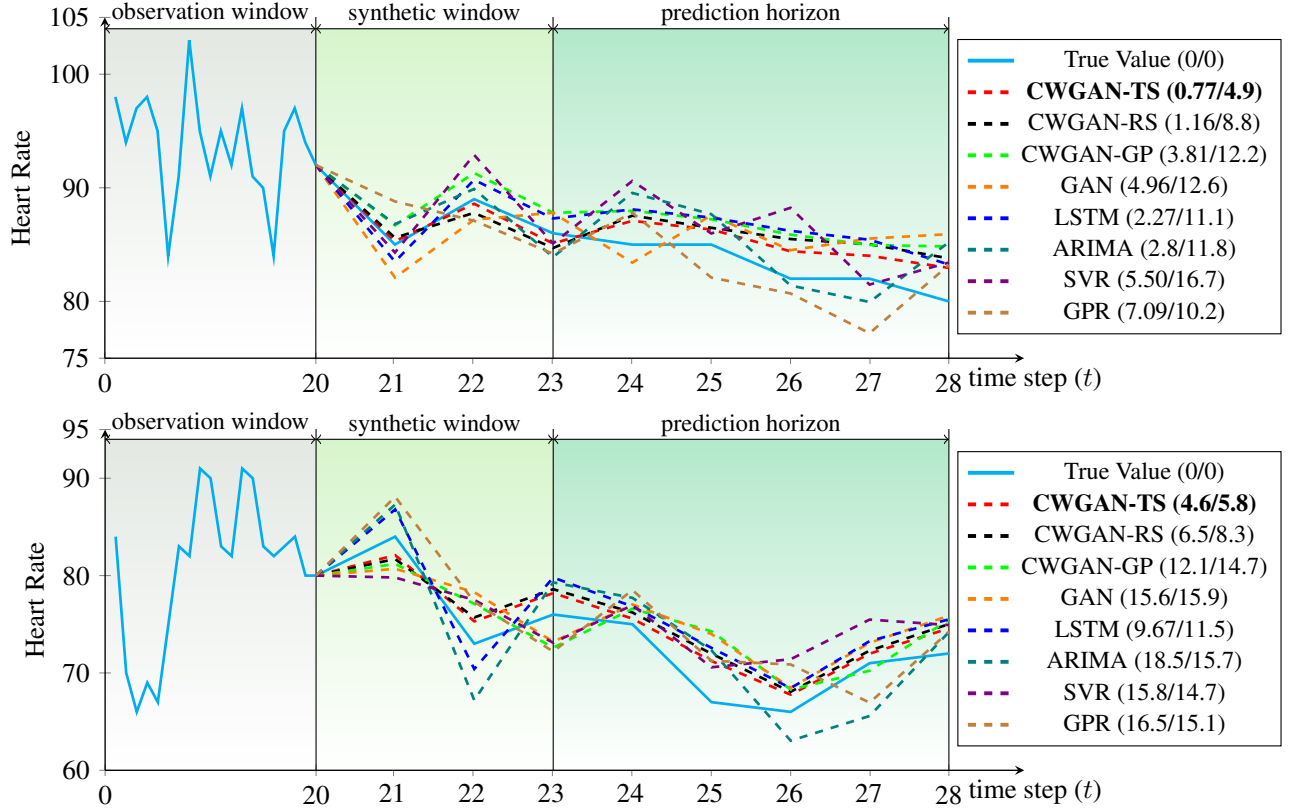


Figure 5: Synthetic data recursively generated by various models and their corresponding forecasting performance based on observed and generated data, for predicting heart rate using the MIMIC-III Vital Signs dataset (Upper: Subject ID 109, lower: Subject ID 890). The values in parentheses are the MSE of the synthetic data generation and the forecasting performance, averaged over the synthetic window and prediction horizon, respectively.

A.4 Ablation Study: Averaged Performance over All Subjects

In this subsection, we study the synthetic data generation performance ($t + 1$ to $t + 3$) and the corresponding forecasting performance ($t + 4$ to $t + 8$) based on observed and synthetic data. Instead of a single subject, we show the averaged performance of all subjects in Table 6. We highlight that the generative performance of CWGAN-TS at $t + 1$ is comparable to or worse than the strong baselines. However, starting from $t + 2$, the generative performance of CWGAN-TS becomes better, leading to better forecasting performance. This demonstrates the superior performance of CWGAN-TS in mitigating error propagation over the strong baselines and its impact on the forecasting performance. Overall, we observe that CWGAN-TS outperforms the best performing benchmark by 5.9% - 9.9% in synthetic data generation and by 5.06% - 10.9% in long-range forecasting.

Performance (MSE)	Generation			Forecasting			
	$t + 1$	$t + 2$	$t + 3$	$t + 4$	$t + 8$	$t + 12$	$t + 24$
ARIMA	106.3	125.7	145.3	160.2	193.2	201.4	225.7
GPR	101.5	119.5	131.4	141.2	175.2	190.4	205.2
SVR	103.2	125.5	134.7	135.2	171.3	192.7	209.3
LSTM	95.2	110.6	127.8	142.8	169.6	187.3	199.4
LSTNet	91.3	107.4	116.8	136.8	164.3	179.4	189.3
TLSTM	90.2	106.5	113.2	129.3	159.4	169.8	185.7
LogSparse	89.3	103.7	114.8	135.3	157.2	171.2	181.7
TimeGAN	94.2	114.3	121.8	139.7	167.9	180.4	195.3
CWGAN-TS	90.7	97.5	101.9	115.2	145.3	161.2	169.4
Min Improvement	-	5.97%	9.98%	10.9%	7.57%	5.06%	6.77%

Table 6: Ablation Study: Averaged results of all subjects in generating/forecasting heart rate using CWGAN-TS and others.

A.5 More Results Using TSCV

We repeated our experiments for predicting NO₂ emission (the Air Quality dataset) using Time Series Cross Validation (TSCV). Specifically, all datasets are split into training set (60%), validation set (20%) and test set (20%) in chronological order to ensure that there is no potential data leakage from using future observations from the other units. We tune all parameters using the validation set (same as Section 4.2) and compare the performance (MSE \pm standard deviation over 5 runs) of using TSCV to Population Informed Cross Validation (PICV) as follows. We can see that the predictive performance becomes slightly different as the training and test data have changed, but the proposed GenF still outperforms the strong baselines by at least 7.8% (compare GenF-2 to LSTNet at $t + 12$).

Prediction Horizon	PICV			TSCV		
	$t + 4$	$t + 8$	$t + 12$	$t + 4$	$t + 8$	$t + 12$
LogSparse	543 \pm 17	851 \pm 23	907 \pm 35	572 \pm 29	855 \pm 19	971 \pm 33
LSTM	548 \pm 13	867 \pm 33	993 \pm 23	603 \pm 22	819 \pm 26	1023 \pm 29
LSTNet	518 \pm 33	827 \pm 28	919 \pm 39	557 \pm 27	790 \pm 25	940 \pm 30
GenF-1	465 \pm 24	715 \pm 31	856 \pm 23	509 \pm 32	688 \pm 25	893 \pm 27
GenF-2	409 \pm 29	669 \pm 27	814 \pm 30	433 \pm 24	593 \pm 29	866 \pm 22

Table 7: Performance comparison between PICV and TSCV using the Multi-Site Air Quality dataset.